J. Fluid Mech. (1978), *vol.* 88, *part* 4, *pp.* 659–684
Printed in Great Britain

An experimental study of the decay of temperature fluctuations in grid-generated turbulence

By Z. WARHAFT AND J. L. LUMLEY

Sibley School of Mechanical and Aerospace Engineering,
Cornell University, Ithaca, New York 14853

(Received 19 July 1977 and in revised form 9 May 1978)

Previous measurements of the decay rate of the fluctuation intensity of passive scalars in grid-generated turbulence show large variation. New results presented here show that the decay rate of passive temperature fluctuations produced by heating the grid is a function of the initial temperature fluctuation intensity. Although a full reason for this is wanting, spectra of the temperature fluctuations show that, by varying the heat applied to the grid, the wavenumber of the maximum in the temperature spectrum changes, *indicating* that the geometry of the thermal fluctuations is being altered in some way. In these experiments the one-dimensional temperature spectrum shows an anomalous $-\frac{5}{3}$ slope. In order to eliminate the dependence of the decay rate of the temperature fluctuations on their intensity, we describe a new way of generating temperature fluctuations by means of placing a heated parallel array of fine wires (a *mandoline*) downstream from the unheated grid. Results of this experiment show that the decay rate of passive thermal fluctuations is uniquely determined by the wavenumber of the initial temperature fluctuations. In this type of flow there appears to be no equilibrium value for the thermal fluctuation decay rate and hence for the mechanical/thermal time-scale ratio since the thermal fluctuation decay rate does not change within the tunnel length, which is the equivalent of nearly one turbulence decay time.

1. Introduction

One of the aims of contemporary turbulence research is to predict the structure and transport characteristics of a scalar in a turbulent flow field. Indeed, for atmospheric flows and for many engineering flows, the prediction of the scalar field, be it temperature, humidity, a pollutant or any other chemical species, is usually the prime objective. It could be conjectured that the extension of our knowledge from the velocity field to the addition of a scalar to this field should be trivial, yet both theoretically and experimentally this problem has proved to be exceedingly difficult, even for the most simple types of flow. This difficulty is partly due to our incomplete knowledge of the velocity field but it is also due to fundamental problems associated with how the random scalar and vector fields are coupled to each other.

We consider here, from an experimental viewpoint, the simplest case of a scalar in a turbulent flow: that of decaying passive temperature fluctuations in approximately isotropic grid-generated turbulence. We restrict our study to incompressible flow, and since the flow medium is air the Prandtl number is of order unity. That such

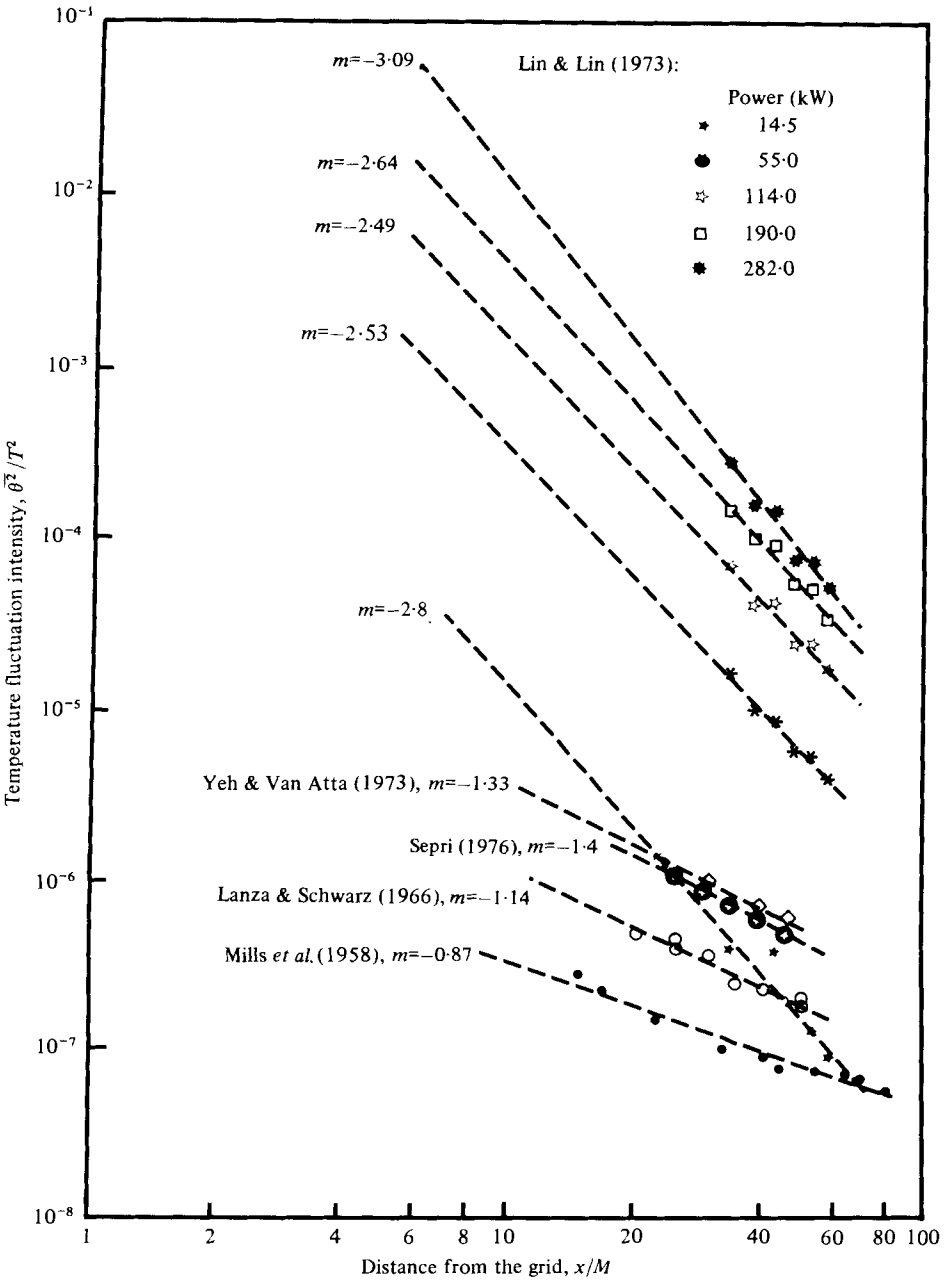

FIGURE 1. Decay of temperature fluctuations downstream of heated grids (after Lin & Lin 1973).

a subject warrants further study is evident from the compilation of previous experimental results shown in figure 1. The decay law for this type of experiment is usually written in the form

$$\overline{\theta^2}/T^2 = B(x/M)^{-m}, \tag{1}$$

where $\overline{\theta^2}$ is the variance of the temperature fluctuations, T is the mean temperature, x/M is the normalized downstream distance, M is the mesh length and B and m are

constants. x is customarily measured from a virtual origin; in these experiments this is within a few M of the grid. For the experimental results shown in figure 1, the decay exponent m varies from 0·87 to 3·1. The approximate trend of increasing m with increasing initial temperature fluctuation intensity may suggest the influence of buoyancy; however, with the possible exception of the highest heating value of Lin & Lin (1973), order-of-magnitude analysis indicates that the buoyancy term in the turbulence energy equation is negligible. For the decay of the velocity fluctuation intensity $\overline{u^2}$, numerous experiments (Comte-Bellot & Corrsin 1966) suggest that the decay exponent n in the decay law

$$\overline{u^2}/U^2 = A(x/M)^{-n}, \tag{2}$$

where U is the mean velocity and A is a constant, is $1{\cdot}3 \pm 0{\cdot}15$. Thus while the velocity intensity decay exponent has a variation of about 12 %, the temperature intensity decay exponent varies by a factor of more than 3. For such flows it would be reasonable to expect that the ratio m/n should be unique.

The significance of the large variation in the decay rate of $\overline{\theta^2}$ is exemplified when we consider characteristic time scales τ and τ_θ for the velocity and thermal fields respectively. We define their ratio r as

$$r = \tau/\tau_\theta = (\overline{q^2}/\epsilon)/(\overline{\theta^2}/\epsilon_\theta), \tag{3}$$

where $\overline{q^2}$ is twice the turbulent kinetic energy, ϵ is the rate of dissipation of kinetic energy and ϵ_θ is the rate of dissipation of half the temperature variance. For grid-generated turbulence, from (1) and (2), $r = m/n$, the ratio of the decay exponents of the temperature and velocity variance. Assuming $n = 1{\cdot}3$, the results in figure 1 give a variation of r from 0·67 to 2·38, an inexplicably large variation for this ratio in a flow in which the controlling time scale would appear to be that of the velocity, which is a constant. The significance of the time-scale ratio r in second-order modelling procedures is discussed by Newman, Launder & Lumley (1978).

The initial objective of this study, then, was to gain an understanding of the reason for the large disparity of the data in figure 1.

2. Outline of the experiment

Our experiment falls into two parts. First we attempted a simulation of the data in figure 1 by doing a heated-grid experiment. We found that it is possible to change the decay rate of $\overline{\theta^2}$ by changing the heat applied to the grid and thus simulated some of the experiments in figure 1. The form of the temperature spectra suggests, however, that by changing the heat applied to the grid we change the length (and hence time) scale of the thermal fluctuations. We then deliberately attempted to change the mechanical/thermal time-scale ratio by heating only alternate bars of the grid. In this experiment too, the decay rate of $\overline{\theta^2}$ was a function of the heat applied to the grid.

In order to introduce temperature fluctuations into the flow in such a manner that their decay rate was not a function of their initial fluctuation intensity we carried out a second experiment. Here we introduced a plane array of parallel, uniformly heated fine wires downstream from the unheated grid. We call this array of wires a *mandoline* because it resembles the French kitchen utensil used to chop and slice vegetables. The wire diameters of the *mandoline* were too fine to shed vortices and hence affect the velocity field. By varying the spacing between the wires and the

distance of the *mandoline* from the grid, we were able to control the input scale of the temperature fluctuations independently of their fluctuation intensity.

Because there is a paucity of information in the literature on the form of temperature spectra in such flows, we document here also a number of three-dimensional normalized energy and dissipation temperature spectra for the different experiments undertaken.

3. Experimental apparatus and procedure

The open-circuit wind tunnel was vertically oriented and had a test section of streamwise extent 167 mesh lengths ($M = 2{\cdot}54$ cm) and cross-section 16 by 16 mesh lengths; it is described by Snyder & Lumley (1971). The mean wind speed U was 6·5 m/s. The solidity of the grid was 0·34; it consisted of a biplane arrangement of 0·476 cm hollow square-sectioned brass rods with their centres spaced 2·54 cm apart. Chromal-A conductors encased in alumina insulators were inserted through the rods and were fed from a 120 V three-phase supply. The heating of the rods was varied by changing the number of rods in series across the power supply. The bars were silver-soldered together at their intersection in order to ensure good thermal homogeneity across the grid. The maximum power consumption was 11·5 kW. For the case when every alternate bar was heated, a second grid was constructed with a slight air gap between the rods at their intersection.

The *mandoline* was made from Chromel-A wire of diameter 0·321 mm. It was verified experimentally that these wires did not affect the velocity fluctuation characteristics of the flow. The wires were oriented in only one direction; their spacing was 5·08 cm and on one occasion 2·54 cm. They were positioned, for the various experiments, at 1·5, 5 and 20 mesh lengths from the grid. To prevent sagging when the wires were heated, small springs were positioned in tension between the ends of the wires and the tunnel wall. Apart from the scientific significance of using a heated *mandoline* rather than a heated grid it should be noted that far less power was required to produce temperature fluctuations. A power consumption of 700 W with the *mandoline* at $x/M = 1{\cdot}5$ produced the same temperature fluctuation intensity as 11·5 kW with the heated grid. Thus the mean temperature of the flow remained close to ambient and problems of large-scale temperature inhomogeneity were avoided.

For all runs, r.m.s. velocity and temperature measurements were made across the core of the flow to check for homogeneity. Irregular variations of about 5 % for the r.m.s. velocity and 7 % for the r.m.s. temperature were measured for both the heated grid (all bars on) and the *mandoline*. For the case of the grid with alternate bars heated, horizontal homogeneity was harder to achieve and on some occasions variations of approximately 12 % occurred in the r.m.s. temperature across the core of the flow. However, on these occasions measurements of the temperature and velocity decay were made for positions other than the centre of the core of the flow, and the variations in the decay rates for different positions in the core were small compared with the gross variation caused by changing the mean power applied to the rods.

For the heated grid the mean temperature of the air in the test section varied from 308 to 300 °K depending on the amount of power used and the variation of the mean temperature between $x/M = 20$ and $x/M = 167$ was less than 0·1 °C. The ambient temperature was approximately 300 °K.

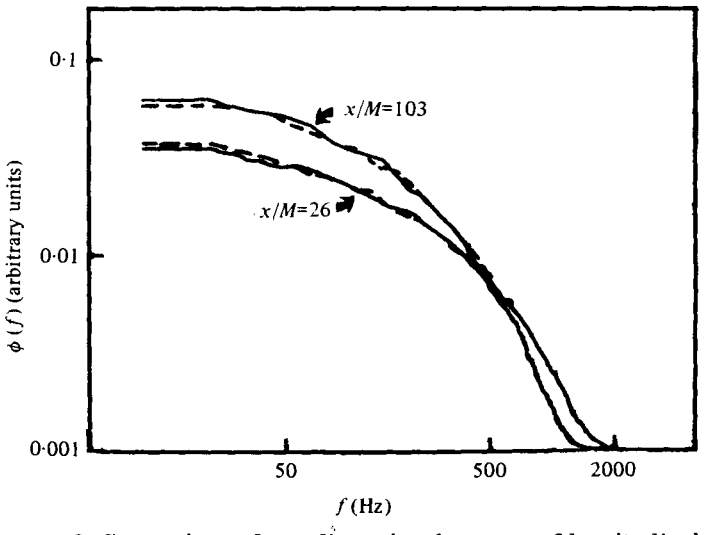

FIGURE 2. Comparison of one-dimensional spectra of longitudinal velocity fluctuations. ———, grid heated; — — —, grid unheated.

Velocity fluctuations were measured with DISA type 55M constant-temperature bridges. An initial set of measurements was made (with the grid both hot and cold) with an X-wire array to obtain the u (longitudinal velocity) and v (lateral velocity) components. For subsequent measurements a single U-wire was used to check that the velocity fluctuation characteristics did not alter. The wires were 3 μm diameter tungsten with a length-to-diameter ratio l/d of 200. The overheat ratio was 1·8. Temperature fluctuations were measured with a fast-response a.c. temperature bridge designed by Mr T. Deaton of the University of California at San Diego. The temperature sensor was 1·27 μm diameter platinum and had l/d = 360.

Velocity fluctuation decay rates and spectra were measured with and without heat applied to the grid (or *mandoline*) and no difference in the decay rate of the fluctuations or in the shape and level of the spectra was observed for the data reported here. Figure 2 shows two such pairs of spectra. Thus we were satisfied that the temperature field was passive.

The current in the temperature probe was kept sufficiently small to ensure that the temperature measurements were not contaminated by velocity fluctuations. As a check for velocity contamination, measurements of 'temperature' were made in the tunnel under isothermal flow conditions (grid cold). The spectrum measured was spiky, indicating some electrical noise, but was of a non-turbulent nature. The r.m.s. voltage did not decrease as a function of downstream distance as it should if there were velocity contamination. Subtraction of this output voltage of the temperature bridge from the temperature measurements deliberately produced by the heated grid or *mandoline*, on a mean-square basis, changed the value of $\overline{\theta^2}/T^2$ by a maximum of 5% at x/M = 167, the position where the lowest temperature fluctuations were produced. This was not a large enough value to change the form of the decay law significantly. The frequency response of our temperature probe was calculated from formulae derived by LaRue, Deaton & Gibson (1975) and was found to be 2·5 kHz, a value well above the Kolmogorov frequency for our experiments.

For the heated-grid experiment the cross-correlation between u and θ was found to be large ($\sim -0{\cdot}3$) and initially we considered that there might be either velocity contamination of the temperature measurements or temperature contamination of the velocity measurements. However, a point-by-point attempt at compensation on our computer did not reduce this correlation. Subsequently we found this high correlation to be due to the method of production of temperature fluctuations by the heated grid. As further confirmation that the velocity and temperature signals were not contaminated by each other, the cross-correlation for the heated *mandoline* was found to be between $-0{\cdot}1$ and $-0{\cdot}05$ for the same level of temperature fluctuations as was produced by the heated grid.

Both temperature and velocity signals were high-pass and low-pass filtered at 1 Hz and 3 kHz respectively through Krohnhite type 3342 filters. The signals were recorded on digital magnetic tape for subsequent playback on a Hewlett–Packard 2100 computer. During the experiment signals were monitored on true-reading r.m.s. meters and spot checks on spectral shape were carried out on a spectrum analyser. The mean velocity was measured with Pitot tubes and the mean temperature with thermocouples. Calibrations were done routinely for each experiment.

The spectra and variances were calculated from between 10^5 and 2×10^5 data points. Larger amounts of data did not change the values to be reported in the next section. Conventional FFT routines were used to form the spectra and these were smoothed by fitting a running second-order polynomial to the raw spectra by the method of least squares. The one exception to this procedure was that used for the spectra in figure 2, which were produced by a hard-wired spectrum analyser.

4. The experimental results

4.1. *The velocity data*

Figure 3 shows the fluctuation intensity of u and v as a function of x/M. The decay exponent n for $\overline{u^2}$ is 1·34, a decay rate in conformity with numerous other experiments at comparable Reynolds numbers (Comte-Bellot & Corrsin 1966). The salient parameters for this flow are listed in table 1. No virtual origin (Comte-Bellot & Corrsin 1966) was needed to fit the best line through these data or any of the temperature fluctuation data to be described in the next subsection. The $\overline{v^2}$ data indicate that the flow was close to isotropic. The one-dimensional power spectra $\phi(k_1)$ of $\overline{q^2}$ ($\equiv\overline{u^2}+2\overline{v^2}$) are shown in figure 4 for three different values of x/M. Figure 5 shows the three-dimensional velocity spectra $E(k)$, where

$$E(k) = -\tfrac{1}{2}k\,d\phi(k)/dk. \tag{4}$$

Here

$$\int_0^\infty \phi(k_1)\,dk_1 \equiv \overline{q^2}.$$

These spectra have been normalized by division by the local values of $\overline{u^2}$ and l, where $l \equiv (\overline{u^2})^{\frac{3}{2}}/\epsilon$. ϵ has been calculated from the velocity decay law and is in good agreement with values calculated by integrating the dissipation spectra. Figure 6 shows the three-dimensional velocity dissipation spectra normalized with the usual Kolmogorov scaling parameters (table 1). Both the energy and the dissipation spectra collapse almost perfectly with the above normalization.

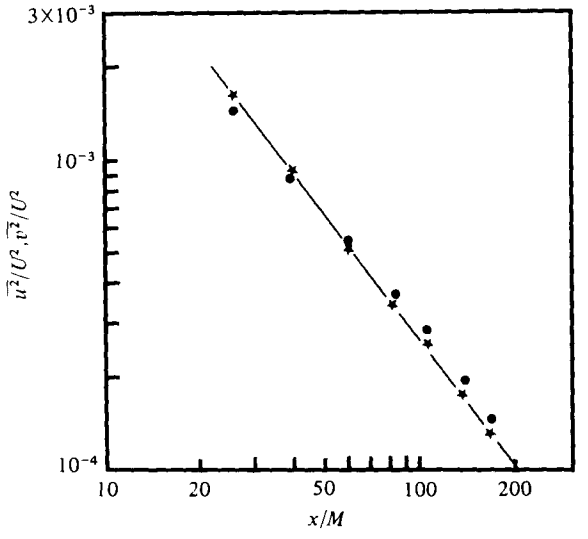

FIGURE 3. Decay of velocity fluctuations downstream of the grid. ★, $\overline{u^2}/U^2$; ●, $\overline{v^2}/U^2$.

ν (m²/s)	$1{\cdot}65 \times 10^{-5}$
U (m/s)	6·5
M (m)	0·0254
$R_M = UM/\nu$	10×10^3
$R_l = q^4/(9\epsilon\nu)$	155
$\overline{u^2}/U^2 = A(x/M)^{-n}$ n	1·34
A	0·1225
$\overline{u^2}$ (m/s)	$1{\cdot}46 \times 10^{-2}$
$l = (\overline{u^2})^{\frac{3}{2}}/\epsilon$ (m)	$1{\cdot}9 \times 10^{-2}$
$\epsilon = -\frac{3}{2}d\overline{u^2}/dt$ (m²/s³)	$9{\cdot}51 \times 10^{-2}$
$\overline{v_k^2} = \nu^{\frac{1}{4}}\epsilon^{\frac{1}{4}}$ (m²/s²)	$1{\cdot}25 \times 10^{-3}$
$k_k = (\epsilon/\nu^3)^{\frac{1}{4}}$ (m⁻¹)	$2{\cdot}15 \times 10^3$

TABLE 1. Velocity flow parameters. The fluctuation parameters are calculated for $x/M = 80$. R_M and R_l are the mesh and turbulence Reynolds numbers respectively.

This basic set of velocity data was reproduced for all the flows with the cold grid, the hot grid and the *mandoline*.

4.2. *The temperature data*

The heated grid. Figure 7 shows the temperature fluctuation intensity as a function of x/M for two different grid heatings. The higher heating gives results close to the data of Yeh & Van Atta (1973) and Sepri (1976). The decay exponent is 1·41. The lower grid heating essentially simulates the data of Mills *et al.* (1958). Here $m = 0{\cdot}83$. The basic parameters for these two heated-grid flows are given in table 2.

Our realization that altering the grid heating changes the decay rate of $\overline{\theta^2}$ suggested that the disparity in decay rates shown in figure 1 may be entirely accounted for by differences in the initial values of the temperature fluctuation intensity. (That this was

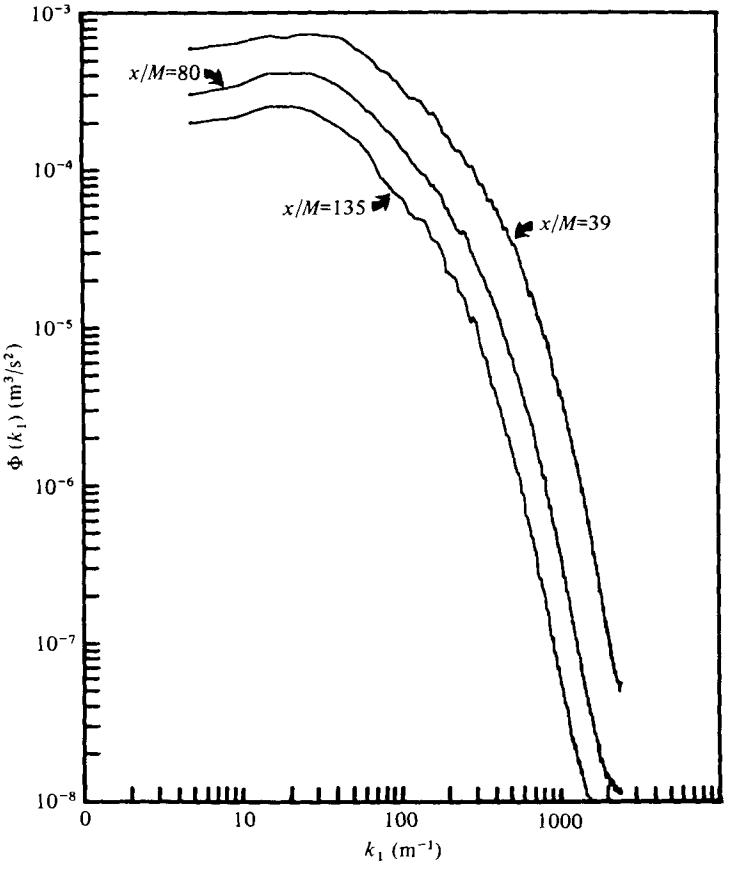

FIGURE 4. One-dimensional spectra of the turbulent energy fluctuations at three different positions downstream from the grid.

not evident to us at the outset is due to two factors: first, the graph in Lin & Lin (1973) contained salinity fluctuation data and did not include the more recent data, thus the trend was less obvious; second, we were reluctant to see a trend in data we believed should yield a unique time scale; we were more concerned that the disparity was due to different experimental set-ups and procedures.) In figure 8 we have plotted the fluctuation intensity $\overline{\theta^2}/T^2$ *vs.* the decay slope for our data and the data in figure 1 at $x/M = 40$ and $x/M = 60$. We have neglected one set of data of Lin & Lin (1973) because of large scatter. The trend in the data (figure 8) is quite remarkable considering the different types of grids and different flow velocities for the different experiments. The coefficient of determination of the line of best fit is 0·95. It should be noted that the difference of about 70 °K between the mean temperatures T for the highest and lowest fluctuation data has an insignificant effect on the trend of the data, which is solely due to variations in $\overline{\theta^2}$.

The fact that the decay rates of these passive temperature fluctuations are functions of their intensity seems to imply that the geometry of the fluctuations is affected by their mode of production at the grid. We have shown in the previous subsection that the velocity field was close to isotropic, and an implicit assumption was that the

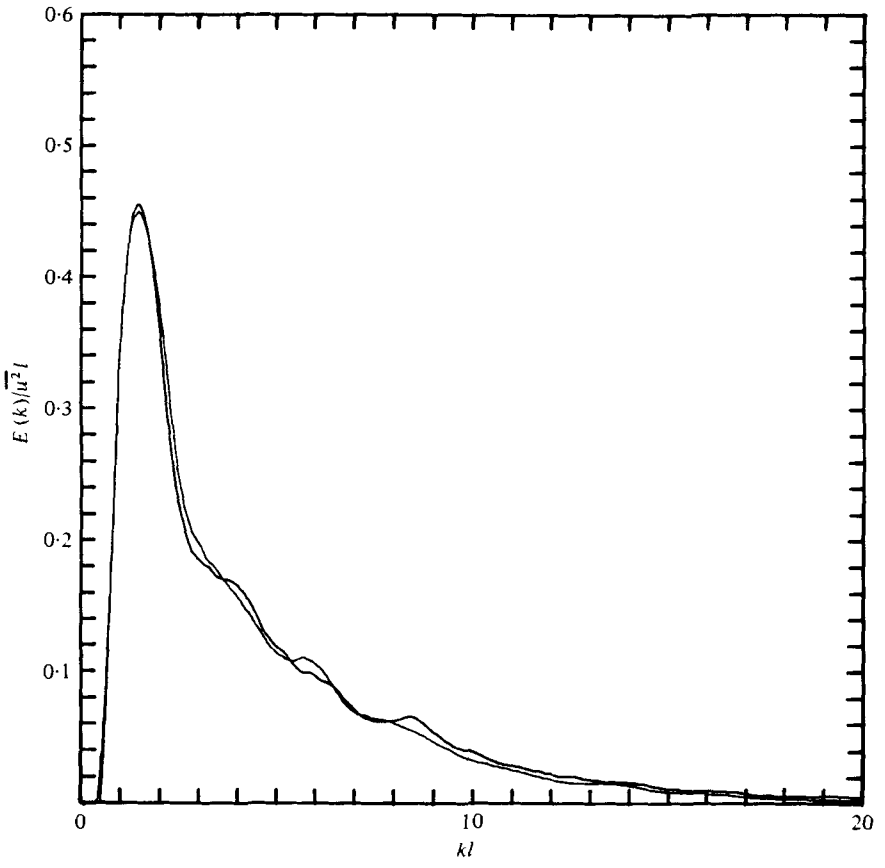

FIGURE 5. Normalized three-dimensional velocity spectra at $x/M = 59$ and $x/M = 80$.

thermal fluctuations would be isotropic also. We did not measure the three-dimensional spectra of temperature fluctuations directly, an extremely difficult task, hence we do not have information on whether the temperature field was isotropic or not. However the one-dimensional energy spectra $k_1 \phi_\theta(k_1)$, where

$$\int_0^\infty \phi_\theta(k_1)\, dk_1 \equiv \overline{\theta^2},$$

for the two grid heatings (shown in figure 9) indicate that if the grid heating is varied the input scale size of the thermal fluctuations also varies. It is possible that the k_2 and k_3 components of the thermal field may also change and that the geometry of the thermal fluctuations produced by the heated grid may be a function of the grid heating. If this is the case, the manner in which the geometry of the temperature fluctuations changes is undoubtedly complex, as consideration of figures 7 and 9 suggests. Figure 9 appears to indicate that as the heating of the grid is increased the characteristic length scale of the thermal fluctuations increases. However, the decay curves shown in figure 7 imply the opposite; here the $\overline{\theta^2}$ decay exponent increases and hence the time scale of the temperature fluctuations decreases as more heating is applied to the grid. This implies a *decrease* in the characteristic length scale. Clearly

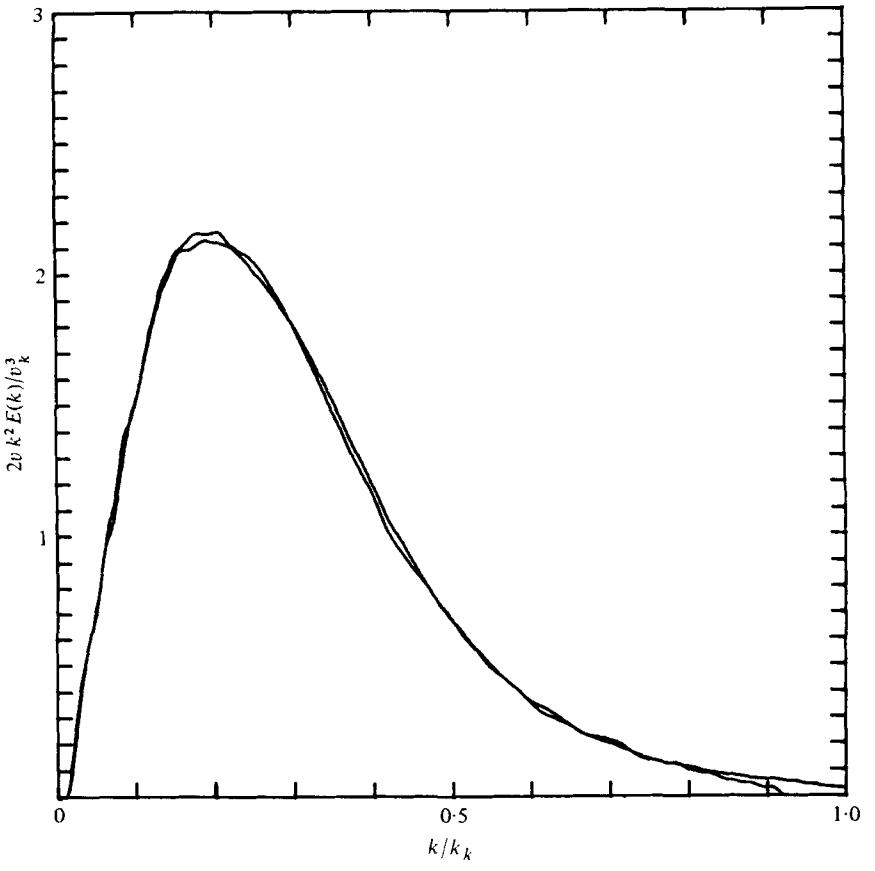

FIGURE 6. Normalized three-dimensional velocity dissipation spectra at $x/M = 59$ and $x/M = 80$.

the spectra in figure 9 can be regarded as only a qualitative indication that the geometry of the thermal field is being affected by the change in grid heating.

A further problem associated with producing temperature fluctuations by means of heating a grid is manifested in the one-dimensional temperature spectra shown in figure 10 for the higher grid heating (the spectra for the lower grid heating were of the same form). Comparing these spectra with the one-dimensional velocity spectra (figure 4), we observe a significant difference in form: the temperature spectra have a linear region with a slope close to $-\frac{5}{3}$ suggestive of an inertial–convective subrange. For heated grids, exactly the same form has been observed by Yeh & Van Atta (1973) and by Sepri (1976). Clearly an inertial–convective subrange cannot occur in such a moderate Reynolds number flow. The reason for this anomalous behaviour in the temperature spectrum appears to be associated with the cross-correlation and coherence between u and θ and will be discussed in the next subsection, where we compare these results with those for the heated *mandoline*. The temperature spectra do, however, collapse well under large-scale normalization and under the assumption of isotropy. Figure 11 shows the three-dimensional temperature spectra

$$E_\theta(k) = -\tfrac{1}{2}k\,d\phi_\theta(k)/dk$$

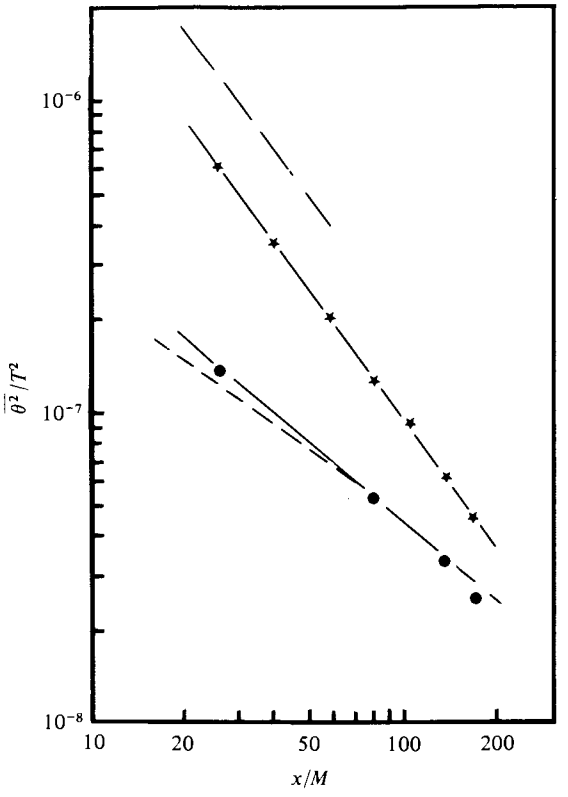

FIGURE 7. Decay of temperature fluctuations downstream of the heated grid for two different grid heatings, ★, 11·5 kW; ●, 2·1 kW; – – –, Yeh & Van Atta (1973); - - - -, Mills *et al.* (1958).

Parameter	Low grid heating (2·1 kW)	High grid heating (11·5 kW)
$\overline{\theta^2}/T^2 = B(x/M)^{-m}\begin{cases} m \\ B \end{cases}$	0·86 $2{\cdot}27 \times 10^{-6}$	1·41 $6{\cdot}19 \times 10^{-5}$
T (°K)	300	308
$\overline{\theta^2}$ (°C²)	$4{\cdot}72 \times 10^{-3}$	$1{\cdot}22 \times 10^{-2}$
$r = m/n$	0·64	1·05
$\epsilon_\theta = -\frac{1}{2}d\overline{\theta^2}/dt$ (°C²/s)	$6{\cdot}49 \times 10^{-3}$	$2{\cdot}79 \times 10^{-2}$
$\overline{\theta_k^2} = \epsilon_\theta(\nu/\epsilon)^{\frac{1}{2}}$ (°C²)	$8{\cdot}55 \times 10^{-5}$	$3{\cdot}67 \times 10^{-4}$

TABLE 2. Temperature parameters for the heated grid at $x/M = 80$. $\overline{\theta^2}$ and ϵ_θ were calculated from the decay laws. A value of $2{\cdot}26 \times 10^{-5}$ was used for ν_θ, the thermal diffusivity.

normalized by $\overline{\theta^2}$ and l. Here, as for other normalized spectra to be discussed below, the difference in magnitude of the peaks does not represent a trend; it represents the maximum scatter observed when other spectra from different positions downstream were collapsed in the same manner. Figure 12 shows the three-dimensional temperature dissipation spectra normalized with Kolmogorov parameters (table 2). These spectra (figures 11 and 12) are for the higher grid heating and are included for comparison with other measurements (Yeh & Van Atta 1973) and with our heated-*mandoline* data.

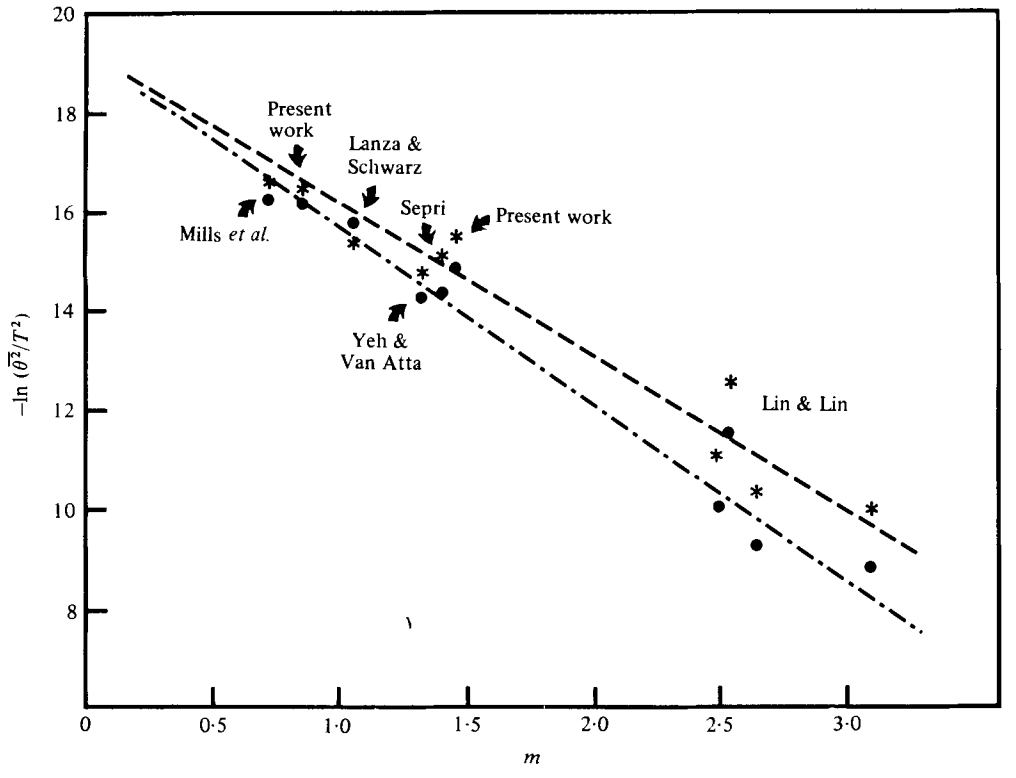

FIGURE 8. Temperature fluctuation intensity $\ln(\overline{\theta^2}/T^2)$ *vs.* decay exponent m for the present work and for previous investigations. ●, $\ln(\overline{\theta^2}/T^2)$ at $x/M = 40$; *, $\ln(\overline{\theta^2}/T^2)$ at $x/M = 60$; —·—, – – –, best fit for $x/M = 40$, 60 (coefficient of determination = 0·95). The lowest grid heating of Lin & Lin (1973) (see figure 1) is not included because of large scatter.

We now briefly mention another experiment with the heated grid which was deliberately aimed at changing the initial length scale of the temperature fluctuations. It was conjectured that, by heating only every alternate bar of the grid, initially the thermal length scale would be twice that of the velocity length scale, i.e. the slope of the $\overline{\theta^2}$ decay law would be less than that of the $\overline{u^2}$ decay law. The results of this experiment show however (figure 13) that even with extremely low temperature fluctuations (cf. the results for low heating with all the bars heated, figure 7) the decay rate achieved was about the same as for the velocity fluctuations, implying a time-scale ratio of about unity. On increasing the power applied to the alternate bars, the decay rate progressively increased (figure 13) and the peaks of the one-dimensional energy spectra (not shown) moved to lower wavenumbers, as for the case where all the bars were heated. We note that it was the result of this experiment, done with various grid heatings because we were having difficulty in obtaining thermal homogeneity, that caused us to vary the heating for the case with all the bars heated.

The heated mandoline. The strong dependence of the decay rate of the temperature fluctuations on the grid heating, with the implication that varying the temperature of the grid might vary the geometry of the thermal field, suggested that we should seek another method of introducing temperature fluctuations into the flow. Use of a

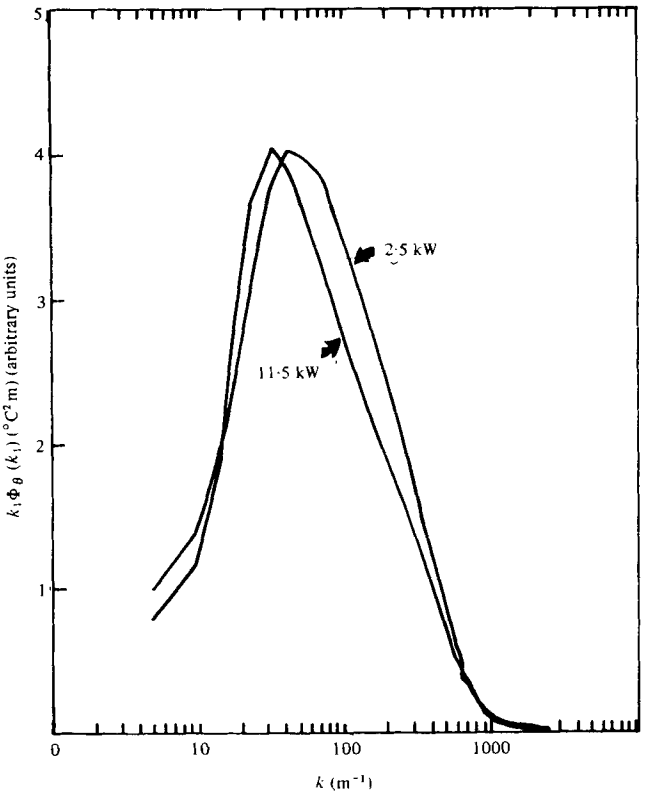

FIGURE 9. One-dimensional temperature spectra at $x/M = 80$ for the two different values of the grid heating. Arbitrary units have been used for the vertical axis in order to compare the wavenumbers at which each spectrum peaks.

mandoline of fine wires placed downstream from the unheated grid, as we shall show, produces results which resolve the problem created by the heated-grid experiment.

Figure 14 shows the decay of temperature fluctuations for four different configurations of the *mandoline*. The origin ($x/M = 0$) was taken at the grid. The configuration data, the decay laws and the relevant scaling parameters for these experiments are summarized in tables 3 and 4.

The decay curves in figure 14 show that, by altering the position of the *mandoline* downstream from the grid and by changing the spacing between the wires of the *mandoline*, we were able to change the decay exponent m from 1·29 to 3·20 without changing the intensity of the thermal fluctuations significantly (the $\overline{\theta^2}/T^2$ values for $x/M = 80$ (table 4) show that the fluctuation intensity varies by less than a factor of two for the four experiments).

Three-dimensional temperature spectra at $x/M = 80$ computed for the different *mandoline* experiments are shown in figure 15. We present these spectra, computed using the isotropic relations, because this is an approximate way of removing aliasing and thus making physical interpretation easier. Since our direct evidence for isotropy is incomplete, however, this should be regarded simply as a convenient transformation. The one-dimensional temperature spectra $k_1\phi_\theta(k_1)$ (not shown here) exhibited the same

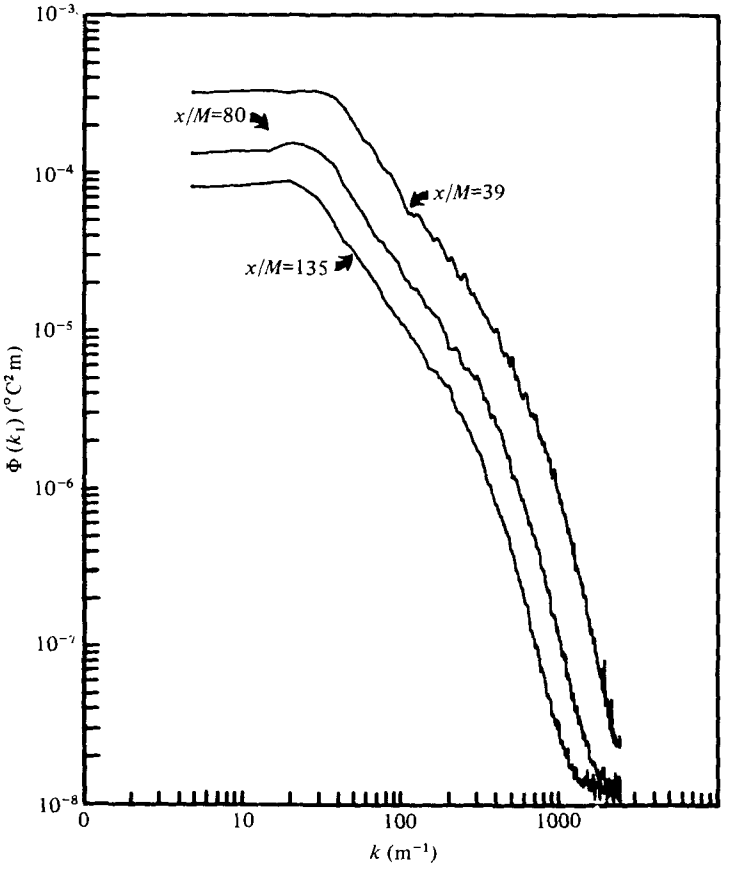

FIGURE 10. One-dimensional spectra of temperature fluctuations at three different distances from the heated grid (11·5 kW).

trend; thus the relationship between the spectral peak and decay rate is not an artifact of this transformation.

Figures 14 and 15 show that as the decay rate increases so does the wavenumber at which the temperature spectrum peaks. It is evident, then, that the decay rate of the temperature fluctuations is *solely* a function of the scale size of the temperature fluctuations for these *mandoline* experiments. Furthermore, faster decay rates of $\overline{\theta^2}$ are associated with higher wavenumbers, i.e. smaller scale sizes, which is an entirely reasonable result, and opposite to that for the heated grid, where faster decay rates appeared to be associated with larger scale sizes.

Figures 14 and 15 are summarized in figure 16, where m and r are plotted as a function of $k_{\max}$, the peak of the respective three-dimensional temperature spectra. The relationship is close to linear. Also shown is the location of the peak of the three-dimensional velocity spectrum, which did not alter for the four experiments. Note that for a time-scale ratio of unity the ratio of the velocity to thermal scale size is 1·24.

Figure 17 compares the one-dimensional temperature spectra for the heated grid and for the heated *mandoline* at $x/M = 80$ (the *mandoline* spectrum is for the 5·04 cm spacing at $x/M = 20$, $m = 2{\cdot}06$). The quasi-inertial-subrange behaviour is not in

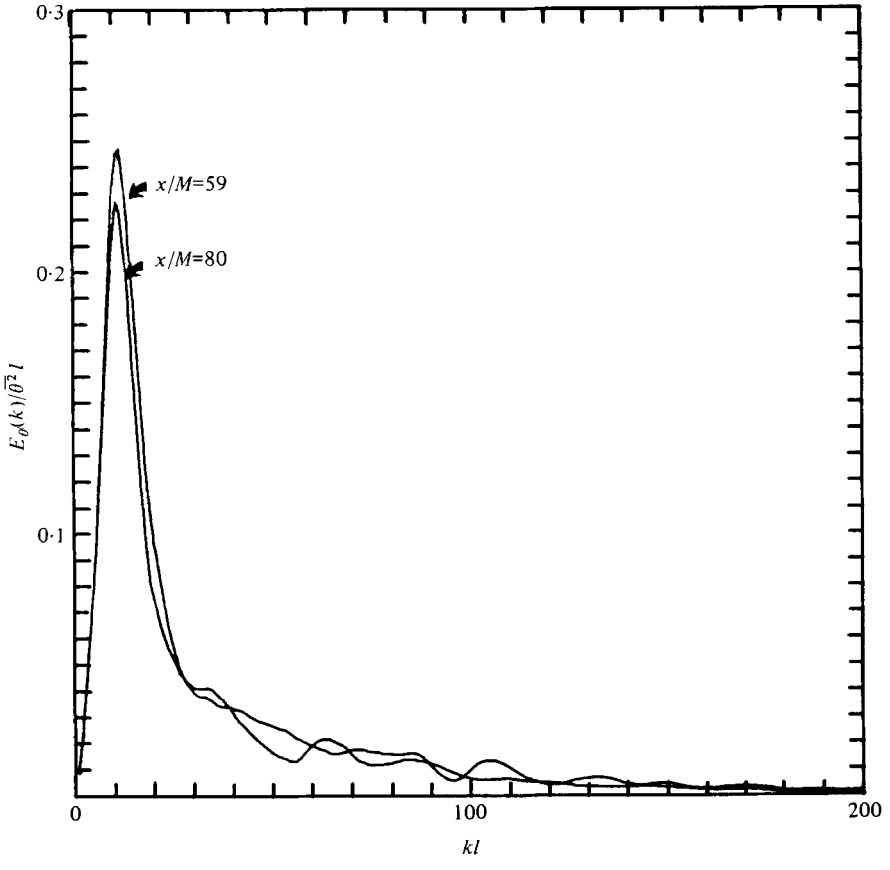

FIGURE 11. Normalized three-dimensional temperature spectra for the heated grid (11·5 kW).

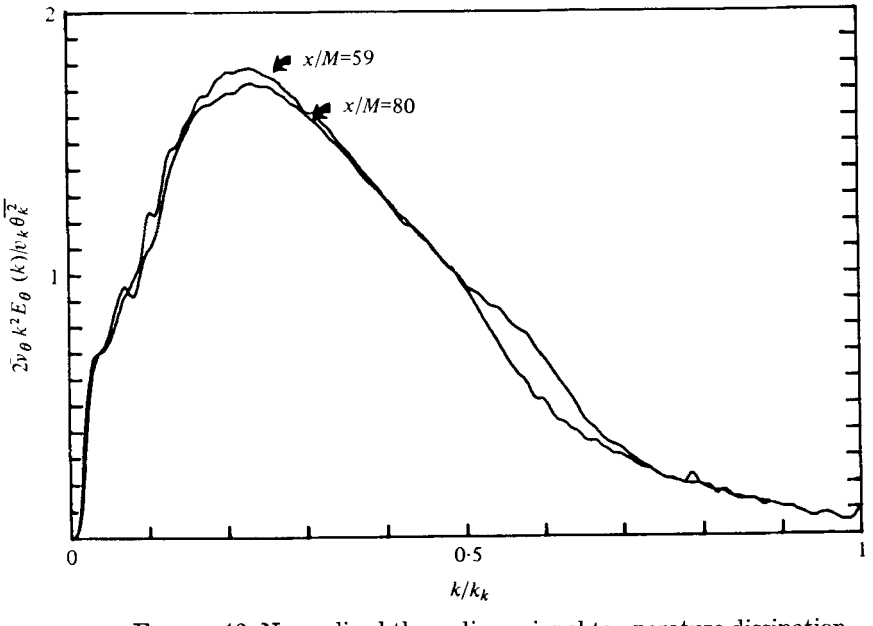

FIGURE 12. Normalized three-dimensional temperature dissipation spectra for the heated grid (11·5 kW).

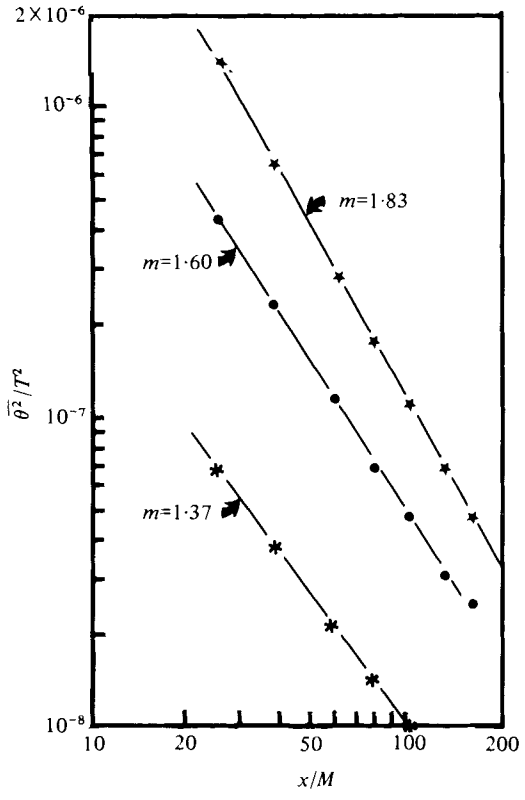

FIGURE 13. Decay of temperature fluctuations downstream from the grid with every alternate bar heated. ★, grid heating 4·2 kW; ●, grid heating 2·5 kW; *, grid heating 0·64 kW.

evidence for the *mandoline* data. The behaviour of the temperature spectra for the heated grid appears to be attributable to the relatively high value of the u, θ coherence $|\phi_{u\theta}(k_1)|^2/\phi_u(k_1)\,\phi_\theta(k_1)$ at low wavenumbers; this coherence is shown in figure 18 with that for the heated *mandoline*. The *mandoline* has low coherence at all wavenumbers. It should be noted that, as the *mandoline* was brought closer to the grid, the linear $-\frac{5}{3}$ portion of the spctrum began to reappear and was quite evident when the *mandoline* was placed at $x/M = 1{\cdot}5$ from the grid. The coherence at low wavenumbers also increased. The cross-correlation coefficients $\rho_{u\theta}$ are plotted as a function of x/M for the *mandoline* and for the heated grid in figure 19. $\rho_{u\theta}$ is greatly reduced for the *mandoline* compared with the heated grid. This large negative $\rho_{u\theta}$ for the heated grid is produced because of the velocity deficit behind the hot bars. $\rho_{u\theta}$ for the heated *mandoline* tends to increase as the *mandoline* is brought closer to the grid, as would be expected, but, even with the *mandoline* at $x/M = 1{\cdot}5$, $\rho_{u\theta}$ is nearly one-third smaller than for the heated grid.

The close-to-linear relation between the peak of the three-dimensional temperature spectra and the decay exponent for the *mandoline* data (figure 16) suggests that the appropriate length scale for these data should be l/r. Figure 20 shows the three-dimensional spectra at $x/M = 51$ and $x/M = 80$ normalized with $\overline{\theta^2}$ and l/r. The collapse is good. This is for the experiment with the *mandoline* at $x/M = 1{\cdot}5$. Figure

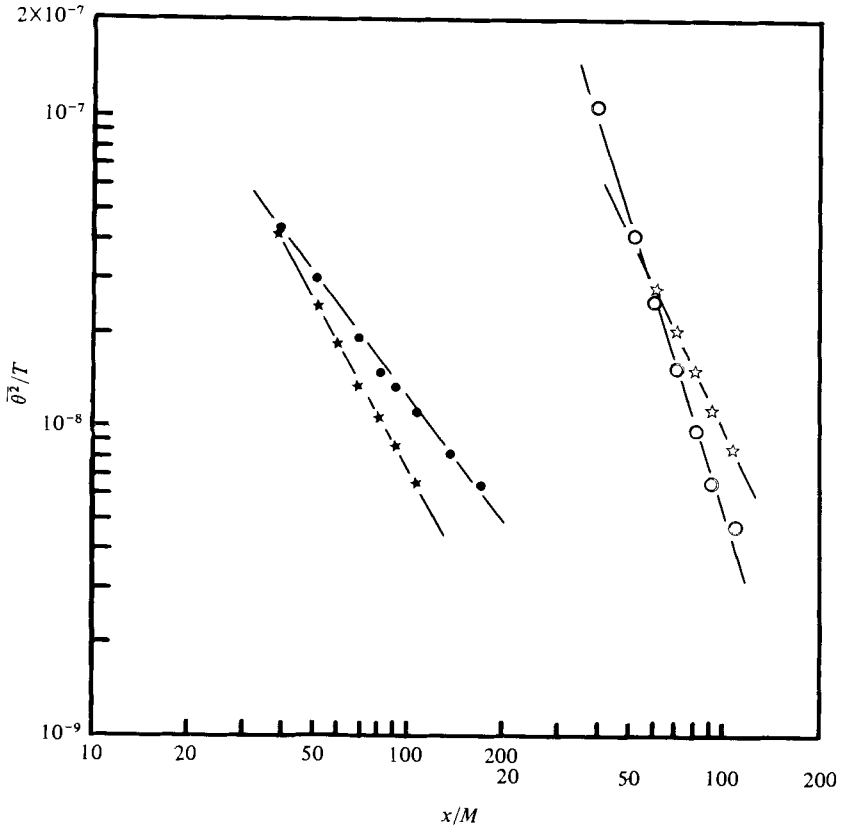

FIGURE 14. Decay of temperature fluctuations downstream from the heated *mandoline*.

	Distance of *mandoline* from grid, x/M	*Mandoline* spacing (cm)	Current in *mandoline* (A)	Decay exponent m
●	1·5	5·08	4	1·29
★	5·0	5·08	2·5	1·83
☆	20·0	5·08	1·5	2·06
○	20·0	2·54	1·5	3·20

Experiment number	Distance of *mandoline* from grid, x/M	Spacing between wires, y/M	Current in wires (A)	Constants in decay law $\overline{\theta^2}/T^2 = B(x/M)^{-m}$	
				B	m
I	1·5	2	4·0	$4{\cdot}65 \times 10^{-6}$	1·29
II	5	2	2·5	$3{\cdot}21 \times 10^{-5}$	1·83
III	20	2	1·5	$1{\cdot}24 \times 10^{-4}$	2·06
IV	20	1	1·5	$1{\cdot}26 \times 10^{-2}$	3·20

TABLE 3. *Mandoline* configuration parameters and decay laws for the four *mandoline* experiments described.

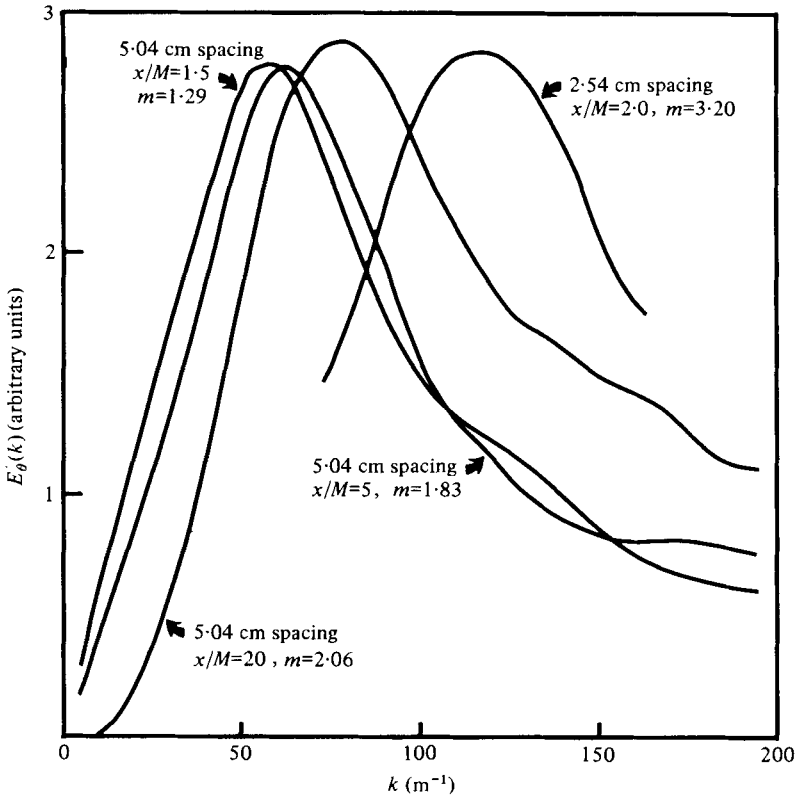

FIGURE 15. Three-dimensional temperature spectra at $x/M = 80$ for the four *mandoline* experiments. Arbitrary units have been used for the vertical axis in order to compare the wavenumbers at which each spectrum peaks.

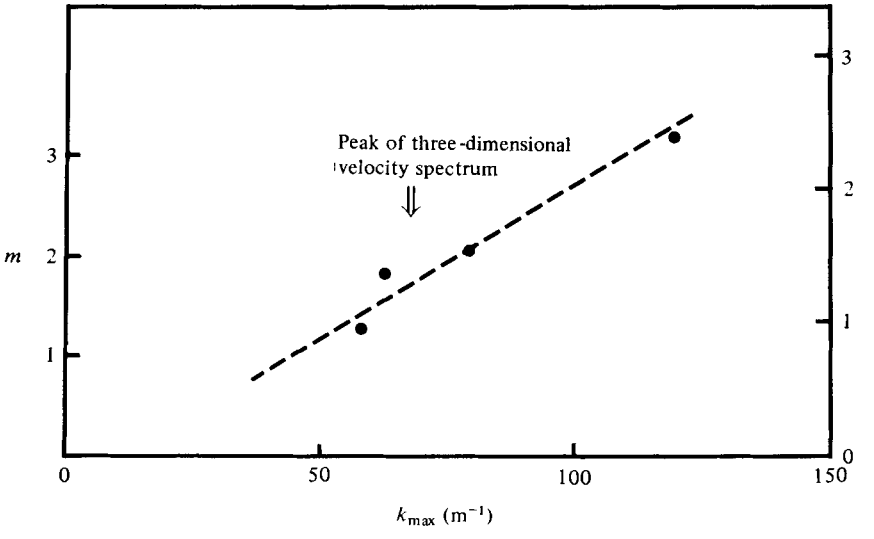

FIGURE 16. The decay slope m and time-scale ratio r of the *mandoline* temperature fluctuation data (from figure 14) *vs.* the peaks of their respective temperature spectra at $x/M = 80$ (from figure 15).

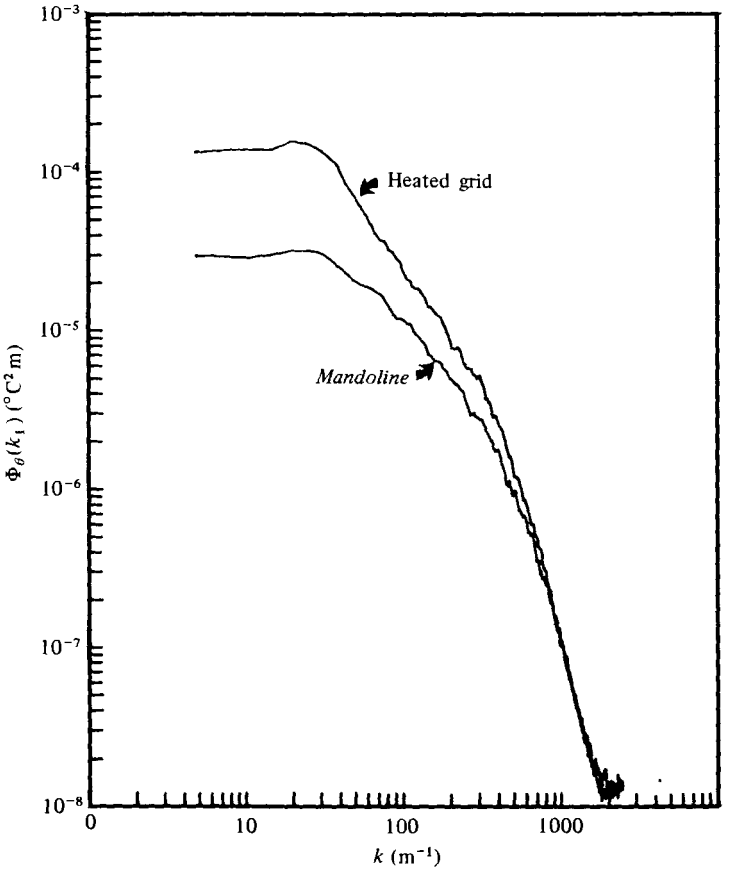

FIGURE 17. Comparison of the one-dimensional temperature spectra at $x/M = 80$ for the heated grid (11·5 kW) and the *mandoline* (5·04 cm spacing, placed at $x/M = 20$ from the grid).

Parameter	Experiment number I	II	III	IV
$\overline{\theta^2}$ (°C²)	$1{\cdot}47 \times 10^{-3}$	$9{\cdot}51 \times 10^{-4}$	$1{\cdot}34 \times 10^{-3}$	$9{\cdot}1 \times 10^{-4}$
$r = m/n$	0·96	1·37	1·54	2·39
$\frac{l}{r} = \frac{(\overline{u^2})^{\frac{3}{2}}}{\epsilon_u} \times \frac{n}{m}$ (m)	$1{\cdot}98 \times 10^{-2}$	$1{\cdot}39 \times 10^{-2}$	$1{\cdot}23 \times 10^{-2}$	$0{\cdot}79 \times 10^{-2}$
$\epsilon_\theta = -\frac{1}{2}d\overline{\theta^2}/dt$ (°C²/s)	$3{\cdot}03 \times 10^{-3}$	$2{\cdot}78 \times 10^{-3}$	$4{\cdot}43 \times 10^{-3}$	$4{\cdot}67 \times 10^{-3}$
$\overline{\theta_k^2} = \epsilon(\nu/\epsilon_u)^{\frac{1}{2}}$ (°C²)	$3{\cdot}99 \times 10^{-5}$	$3{\cdot}48 \times 10^{-5}$	$7{\cdot}84 \times 10^{-5}$	$6{\cdot}15 \times 10^{-5}$

TABLE 4. Temperature parameters for the *mandolines* calculated at $x/M = 80$ from the grid. $T = 300$ °K for all experiments. θ_2^2, ϵ_θ, etc. were calculated from the decay laws. A value of $2{\cdot}26 \times 10^{-5}$ m²/s was used for ν_θ, the thermal diffusivity.

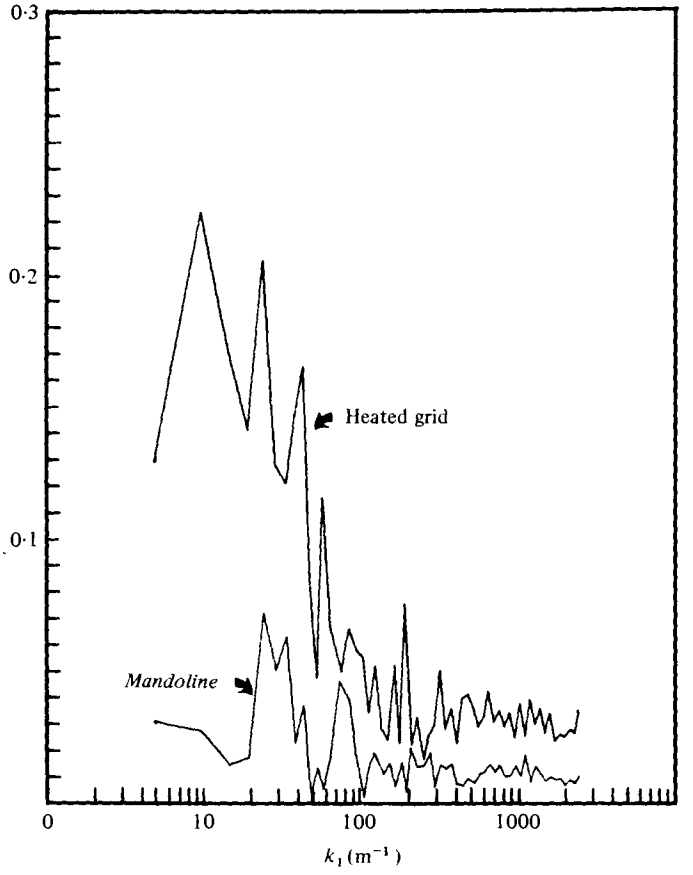

FIGURE 18. Coherence of u and θ at $x/M = 80$ for the heated grid (11·5 kW) and the *mandoline* (5·04 cm spacing, placed at $x/M = 20$ from the grid).

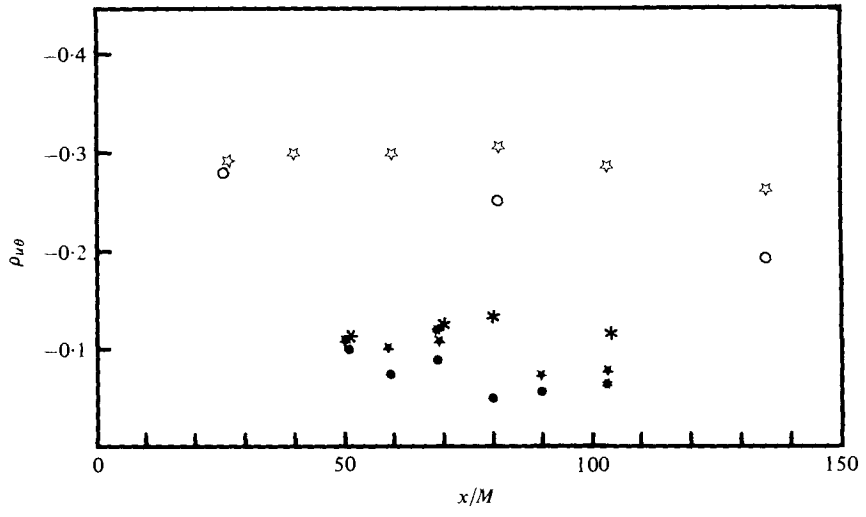

FIGURE 19. Cross-correlation between u and θ as a function of x/M for the heated grid and *mandoline*. ☆, heated grid, 11·5 kW; ○, heated grid, 2·1 kW; ●, *mandoline* at $x/M = 20$, 2·54 cm spacing; ★, *mandoline* at $x/M = 20$, 5·08 cm spacing; ✱, *mandoline* at $x/M = 5$, 5·08 cm spacing; *, *mandoline* at $x/M = 1·5$, 5·08 cm spacing.

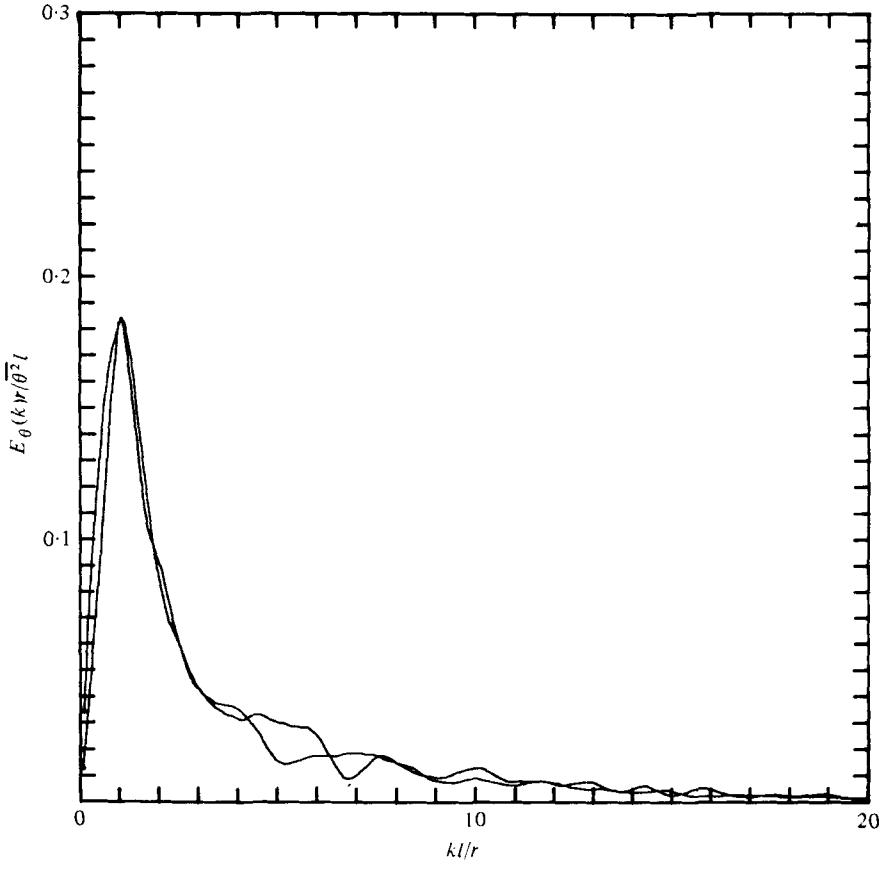

FIGURE 20. Normalized three-dimensional temperature spectra at $x/M = 51$ and $x/M = 103$ for the *mandoline* (5·04 cm spacing, placed at $x/M = 1{\cdot}5$ from the grid).

21 shows that all the *mandoline* data at $x/M = 80$ collapse reasonably well with this normalization; the scatter is due to the slight departure of some points from the linear relation suggested by figure 16.

Finally we present the three-dimensional dissipation spectra of temperature for the *mandoline* experiments for which $m = 1{\cdot}29$ (figure 22) and $m = 2{\cdot}06$ (figure 23). The peaking of the spectra for $m = 1{\cdot}29$ at a slightly lower wavenumber than those for $m = 2{\cdot}06$ reflects the respective positions of the peaks of the three-dimensional temperature spectra (figures 15 and 16). The differences between the two spectra shown in figures 22 and 23 represent scatter and not a trend in the spectral shape with downstream distance.

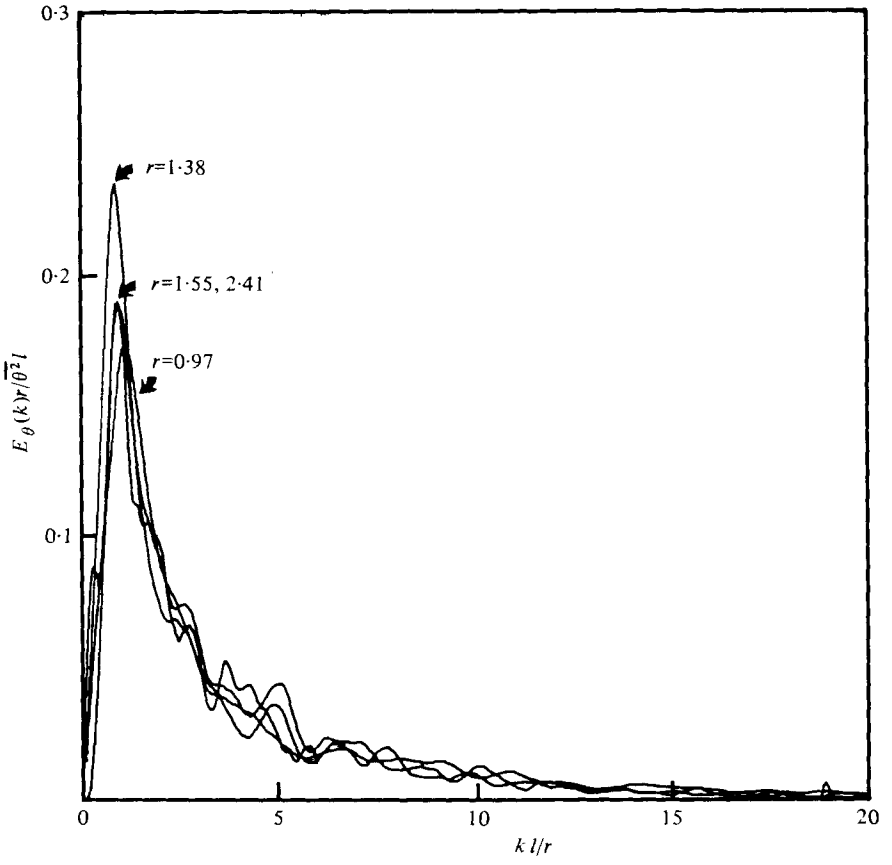

FIGURE 21. Normalized three-dimensional temperature spectra at $x/M = 80$ for all four *mandoline* experiments.

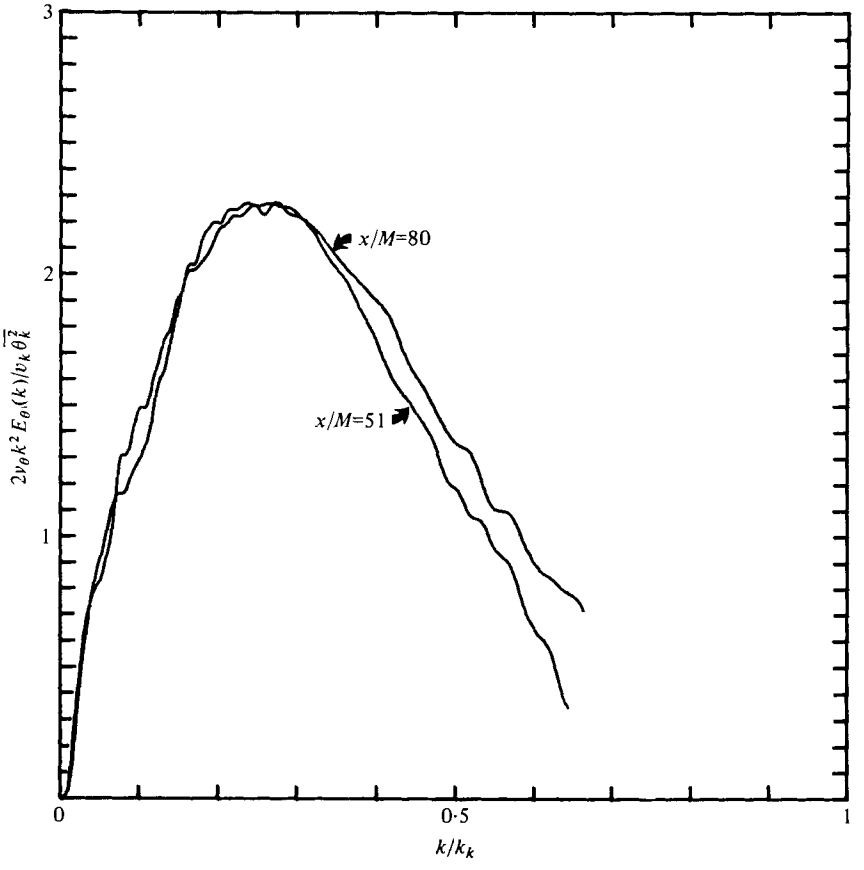

FIGURE 22. Normalized three-dimensional temperature dissipation spectra for the *mandoline* (5·04 cm spacing, placed at $x/M = 1{\cdot}5$ from the grid, $m = 1{\cdot}29$).

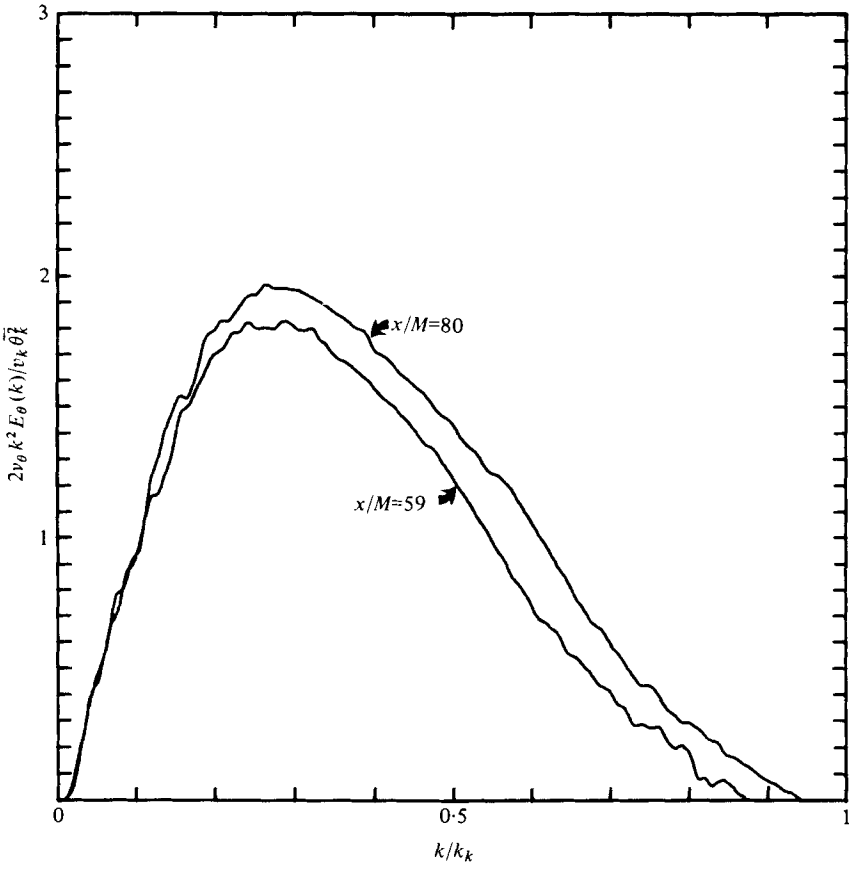

FIGURE 23. Normalized three-dimensional temperature dissipation spectra for the *mandoline* (5·04 cm spacing, placed at $x/M = 20$ from the grid, $m = 2{\cdot}06$).

5. Concluding remarks

The heated-grid data pose problems. We have stated that buoyancy was not playing a role in determining the $\overline{\theta^2}$ decay rate, that the velocity characteristics remained the same as for the unheated grid and that the ratio $(g/T)\ (\overline{u\theta}/\epsilon)$ was of order 10^{-3}, indicating the insignificance of buoyancy compared with dissipation. However the shifting of the peak in the temperature spectrum (figure 9) as the grid heating is changed indicates that the geometry of the thermal field changes. This has led us to conclude that anisotropy may be the cause of the variation of $\overline{\theta^2}$ decay with grid heating. If this is the case its effect is profound, changing the $\overline{\theta^2}$ decay exponent by a factor of nearly two for our experiments and by a factor of 3·5 for the experiments in figure 1. Yet if anisotropy is playing a role it could be supposed that it should be also a function of the grid geometry. The grid of Lin & Lin (1973) consists of a complex structure of heating elements and flow channels and has a high effective solidity, probably producing jets rather than wakes as is the case for heated grids of lower solidity. Yet their data, as well as all the other data, show a very high correlation of fluctuation intensity *vs.* decay slope (figure 8), suggesting that the grid structure is

not playing a role. This problem, and the problem of how the change in grid heating is affecting the thermal length scale without apparently affecting the velocity field, requires further investigation.

The heated-*mandoline* experiments pose the question: is there an equilibrium value for the mechanical/thermal time-scale ratio? Our results suggest not; we find no evidence of the relaxation of r from its initial value to an equilibrium value in our wind tunnel, which extends to nearly one turbulence decay time. Recently, Newman & Herring (1978) have addressed this problem by applying the test-field model of Kraichnan (1971) to the decay of a passive scalar in isotropic turbulence. They find that in less than one turbulence decay time the time-scale ratio relaxes back to a value of unity whatever the initial value was. Possibly the time-scale ratio relaxes to an equilibrium value only in the presence of some other non-equilibrium such as the non-equilibrium in spectral transfer present in the TFM simulations caused by the establishment of spectral transfer which is initially zero. It is pleasing, however, to note that Newman & Herring find that the temperature spectrum peaks at a length scale greater than the velocity length scale for $r = 1$, in qualitative agreement with our results for $r = 1$. It should be noted that both the heated-grid data of Yeh & Van Atta (1973) and our heated-grid data for higher grid heating (11·5 kW) also give $r = 1$ and that the ratio of the length scales of the velocity and temperature spectra is in reasonable agreement with the prediction of Newman & Herring. The grid heating chosen for these experiments appears to be fortuitous; as previously noted, for our lower grid heating the change in length scale (compared with that for the higher grid heating) obtained from the peak in the one-dimensional spectrum is not commensurate with the change in length scale deduced from the $\overline{\theta^2}$ decay law.

We believe that our results should have ramifications for other non-equilibrium flows containing a scalar, for example flows in which chemical reaction rates are a function of the scalar fluctuation intensity or the formation and dissipation of clear-air turbulence. In these flows the scalar may not be passive but it is reasonable to expect that here too the destruction of scalar fluctuations (and their flux) should be a function of the initial relative scale sizes of the velocity and temperature field.

We thank Mr E. P. Jordan for his diligent experimental assistance and Mr G. R. Newman for provocative discussions. This work was supported in part by grant no. DES76-13357/ATM75 13357-A01 from the U.S. National Science Foundation, Atmospheric Sciences Section, and in part by the U.S. Environmental Protection Agency through its Select Research Group in Air Pollution Meteorology, and was carried out at the Pennsylvania State University at University Park in the Department of Aerospace Engineering.

REFERENCES

Comte-Bellot, G. & Corrsin, S. 1966 The use of a contraction to improve the isotropy of grid-generated turbulence. *J. Fluid Mech.* **25**, 657–682.

Kraichnan, R. H. 1971 An almost-Markovian Galilean-invariant turbulence model. *J. Fluid Mech.* **47**, 525–535.

LaRue, J. C., Deaton, T. & Gibson, C. H. 1975 Measurement of high-frequency turbulent temperature. *Rev. Sci. Instrum.* **46**, 757–764.

Lin, S. C. & Lin, S. C. 1973 Study of strong temperature mixing in subsonic grid turbulence. *Phys. Fluids* **16**, 1587–1598.

MILLS, R. R., KISTLER, A. L., O'BRIEN, V. & CORRSIN, S. 1958 Turbulence and temperature fluctuations behind a heated grid. *N.A.C.A. Tech. Note* no. 4288.

NEWMAN, G. R. & HERRING, J. 1978 Second-order modelling and statistical-theory modelling of a homogeneous turbulence. To be submitted to *J. Fluid Mech.*

NEWMAN, G. R., LAUNDER, B. E. & LUMLEY, J. L. 1978 Modelling the behaviour of homogeneous scalar turbulence. To be submitted to *J. Fluid Mech.*

SEPRI, P. 1976 Two-point turbulence measurements downstream of a heated grid. *Phys. Fluids* **19**, 1876–1884.

SNYDER, W. H. & LUMLEY, J. L. 1971 Some measurements of particle velocity autocorrelation functions in a turbulent flow. *J. Fluid Mech.* **48**, 41–71.

YEH, T. T. & VAN ATTA, C. W. 1973 Spectral transfer of scalar and velocity fields in heated-grid turbulence. *J. Fluid Mech.* **58**, 233–261.